Full title: Lip-reading enables the brain to synthesize auditory features of unknown silent speech.

Running title: Synthesizing auditory features of silent speech.

Authors: Mathieu Bourguignon[1,2,3,*], Martijn Baart[1,4], Efthymia C. Kapnoula[1], Nicola Molinaro[1,5]

Affiliations

[1]BCBL. Basque Center on Cognition, Brain and Language, 20009 San Sebastian, Spain.

[2]Laboratoire de Cartographie fonctionnelle du Cerveau, UNI – ULB Neuroscience Institute, Université libre de Bruxelles (ULB), Brussels, Belgium.

[3]Laboratoire Cognition Langage et Développement, UNI – ULB Neuroscience Institute, Université libre de Bruxelles (ULB), Brussels, Belgium.

[4]Department of Cognitive Neuropsychology, Tilburg University, Tilburg, the Netherlands.

[5]Ikerbasque, Basque Foundation for Science, Bilbao, Spain.

*Corresponding author. E-mail: mabourgu@ulb.ac.be.

Number of pages: 47, **number of figures**: 9, **number of tables**: 1, **number of words in *Abstract***: 250, **number of words in *Introduction***: 624, **number of words in *Discussion***: 1490.

Conflict of interest

The authors have no conflict of interest to declare.

Acknowledgment

Mathieu Bourguignon was supported by the Innoviris Attract program (grant 2015-BB2B-10), by the Spanish Ministry of Economy and Competitiveness (grant PSI2016-77175-P), and by the Marie Skłodowska-Curie Action of the European Commission (grant 743562). Martijn Baart was supported by the Netherlands Organization for Scientific Research (NWO, VENI

grant 275-89-027). Efthymia C. Kapnoula was supported by the Spanish Ministry of Economy and Competitiveness, through the Juan de la Cierva-Formación fellowship, and by the Spanish Ministry of Economy and Competitiveness (grant PSI2017-82563-P). Nicola Molinaro was supported by the Spanish Ministry of Science, Innovation and Universities (grant RTI2018-096311-B-I00), the Agencia Estatal de Investigación (AEI), the Fondo Europeo de Desarrollo Regional (FEDER) and by the Basque government (grant PI_2016_1_0014). The authors acknowledge financial support from the Spanish Ministry of Economy and Competitiveness, through the "Severo Ochoa" Programme for Centres/Units of Excellence in R&D" (SEV□2015□490) awarded to the BCBL.

We thank Riitta Hari at Department of Art (Aalto University School of Arts, Design, and Architecture, Espoo, Finland) for helpful comments on the manuscript.

Abstract

Lip-reading is crucial for understanding speech in challenging conditions. But how the brain extracts meaning from—silent—visual speech is still under debate. Lip-reading in silence activates the auditory cortices, but it is not known whether such activation reflects immediate synthesis of the corresponding auditory stimulus or imagery of unrelated sounds.

To disentangle these possibilities, we used magnetoencephalography to evaluate how cortical activity in 28 healthy adults humans (17 females) entrained to the auditory speech envelope and lip movements (mouth opening) when listening to a spoken story without visual input (*audio-only*), and when seeing a silent video of a speaker articulating another story (*video-only*).

In *video-only*, auditory cortical activity entrained to the absent auditory signal at frequencies below 1 Hz more than to the seen lip movements. This entrainment process was characterized by an auditory-speech–to–brain delay of ~70 ms in the left hemisphere, compared to ~20 ms in *audio-only*. Entrainment to mouth opening was found in the right angular gyrus at below 1 Hz, and in early visual cortices at 1–8 Hz.

These findings demonstrate that the brain can use a silent lip-read signal to synthesize a coarse-grained auditory speech representation in early auditory cortices. Our data indicate the following underlying oscillatory mechanism: Seeing lip movements first modulates neuronal activity in early visual cortices at frequencies that match articulatory lip movements; the right angular gyrus then extracts slower features of lip movements, mapping them onto the corresponding speech sound features; this information is fed to auditory cortices, most likely facilitating speech parsing.

Significance statement

Lip-reading consists in decoding speech based on visual information derived from observation of a speaker's articulatory facial gestures. Lip reading is known to improve auditory speech understanding, especially when speech is degraded. Interestingly, lip-reading in silence still activates the auditory cortices, even when participants do not know what the absent auditory signal should be. However, it was uncertain what such activation reflected. Here, using magnetoencephalographic recordings, we demonstrate it reflects fast synthesis of the auditory stimulus rather than mental imagery of unrelated—speech or non-speech—sounds. Our results also shed light on the oscillatory dynamics underlying lip-reading.

Keywords

Lip reading; silent speech; audiovisual integration; speech entrainment; magnetoencephalography

Introduction

In everyday situations, seeing a speaker's articulatory mouth gestures, here referred to as lip-reading or visual speech, can help us decode the auditory speech signal (Sumby and Pollack, 1954). In fact, lip movements are intelligible even without an auditory signal, likely because there is a strong connection between auditory and visual speech (Munhall and Vatikiotis-Bateson, 2004; Chandrasekaran et al., 2009). It is however not clear how the brain extracts meaning from visual speech.

Some evidence points to the possibility that visual speech is recoded into acoustic information. For example, seeing silent visual speech clips of simple speech sounds such as vowels or elementary words activates auditory cortical areas (Calvert et al., 1997; Pekkola et al., 2005), even when participants are not aware of what the absent auditory input should be (Calvert et al., 1997; Bernstein et al., 2002; Paulesu et al., 2003). However, recoding visual speech into an acoustic representation (here referred to as synthesis) is computationally demanding. It has therefore been suggested that meaning is directly extracted from visual speech within visual areas and heteromodal association cortices (Bernstein and Liebenthal, 2014; O'Sullivan et al., 2016; Lazard and Giraud, 2017; Hauswald et al., 2018). According to this view, activation in early auditory cortices driven by lip reading might reflect imagery of unrelated—speech—sounds (Bernstein and Liebenthal, 2014), but not a direct recoding of visual speech into its corresponding acoustic representation. As previous work has relied on time-insensitive neuroimaging techniques (Calvert et al., 1997; Bernstein et al., 2002; Paulesu et al., 2003; Pekkola et al., 2005), there was no empirical evidence to disentangle these two alternatives. Here, we took advantage of auditory cortical entrainment to look for decisive evidence to support the existence of a synthesis mechanism whereby visual speech is recoded into its corresponding auditory information.

When people listen to continuous natural speech, oscillatory cortical activity synchronises with the auditory temporal speech envelope (Luo and Poeppel, 2007; Bourguignon et al., 2012; Gross et al., 2013; Peelle et al., 2013; Molinaro et al., 2016; Vander Ghinst et al., 2016; Meyer et al., 2017; Meyer and Gumbert, 2018). Such "speech-brain entrainment" originates mainly in auditory cortices at frequencies matching phrase (below 1 Hz) and syllable rates (4–8 Hz), and is thought to be essential for speech comprehension (Ahissar et al., 2001; Luo and Poeppel, 2007; Peelle et al., 2013; Ding et al., 2016; Meyer et al., 2017). An electroencephalography study suggested that silent lip-read information entrains cortical activity at syllable rate when participants are highly familiar with speech content (Crosse et al., 2015). However, since participants knew what the absent speech sound should be in this study, it remains unclear whether entrainment is driven by the (i) lip-read information, (ii) covert production or repetition of the speech segment, (iii) top-down lexical and semantic processes, or (iv) some combination of these factors.

Here, we address the following critical question: does the brain use lip-read input to bring auditory cortices to entrain to the audio speech signal even when there is no physical speech sound and participants do not know the content of the absent auditory signal? To do so, we evaluated entrainment to a spoken story without visual input (*audio-only*), and compared these data to a silent condition with a video of a speaker articulating another story (*video-only*). To determine the 'lip-read specificity' of these entrainment patterns, we also included a condition in which the mouth configuration of the speaker telling another story was transduced into a dynamic luminance contrast (*control-video-only*). If the brain can synthesize properties of missing speech based on concurrent lip-reading in a timely manner, auditory cortical entrainment with the envelope of the audio signal should be similar in *audio-only* and *video-only*, even if the speech sound was not physically present in the latter condition.

Materials and Methods

Participants

Twenty-eight healthy human adults (17 females) aged 24.1±4.0 years (mean ± SD) were included in the study. All reported being native speakers of Spanish and right-handed. They had normal or corrected-to-normal vision and normal hearing, had no prior history of neurological or psychiatric disorders, and were not taking any medication or substance that could influence the nervous system.

The experiment was approved by the BCBL Ethics Review Board and complied with the guidelines of the Helsinki Declaration. Written informed consent was obtained from all participants prior to testing.

Experimental paradigm

Figure 1 presents stimulus examples and excerpts. The stimuli were derived from 8 audio-visual recordings of a female native Spanish speaker talking for 5 min about a given topic (animals, books, food, holidays, movies, music, social media, and sports). Video and audio were simultaneously recorded using a digital camera (Canon Legria HF G10) with an internal microphone. Video recordings were framed as head shots, and recorded at the PAL standard of 25 frames per second (videos were 1920 × 1080 pixels in size, 24 bits/pixel, with an auditory sampling rate of 44100 Hz). The camera was placed ~70 cm away from the speaker, and the face spanned about half of the vertical field of view. Final images were resized to a resolution of 1024 × 768 pixels.

For each video, a "control" video was created in which mouth movements were transduced into luminance changes (Fig. 1C). To achieve this we extracted lip contours from each individual frame of the video recordings with an in-house Matlab code based on the

153 approach of Eveno et al. (2004). In the control video, the luminance of a Greek cross changed
154 according to mouth configuration (Fig. 1C). Its size (300 × 300 pixels) was roughly matched
155 with the extent of the eyes and mouth, which are the parts of the face people tend to look at
156 when watching a speaker's face (Vatikiotis-Bateson et al., 1998). Mouth configuration
157 variables (mouth opening, width, and surface) were rescaled so that their 1st and 99th
158 percentiles corresponded to the minimum and maximum luminance levels. The center of the
159 cross encoded the mouth surface area, its top and bottom portions encoded mouth opening,
160 and its left- and rightmost portions encoded mouth width. In this configuration, the three
161 represented parameters were spatially and temporally congruent with the portion of the mouth
162 they parametrized. All portions were smoothly connected by buffers along which the weight
163 of the encoded parameters varied as a squared cosine. These control videos were designed to
164 determine if effects were specific to lip-reading. The transduced format was preferred to other
165 classical controls such as meaningless lip movements or gum-chewing motions because
166 preserved the temporal relation between the visual input and underlying speech sounds.
167 For each sound recording, we derived a non-speech "control" audio consisting of
168 white noise modulated by the auditory speech envelope. These control sounds were designed
169 to determine whether uncovered effects were specific to speech. However, conditions that
170 included these control sounds were not analyzed because they were uninformative about lip-
171 reading driven oscillatory entrainment.
172 In total, participants completed 10 experimental conditions while sitting with their
173 head in a MEG helmet. This included all 9 possible combinations of 3 types of visual stimuli
174 (original, control, no video) and 3 types of audio stimuli (original, control, no audio). The test
175 condition with no audio and no video was trivially labeled as the *rest* condition and lasted 5
176 min. Each of the other 8 conditions was assigned to 1 of the 8 stories (condition–story
177 assignment counterbalanced across participants). In this way, we ensured that each condition

was presented continuously for 5 min, and that the same story was never presented twice. The tenth condition was a localizer condition in which participants attended 400-Hz pure tones and checkerboard pattern reversals lasting 10 min. This condition is not analyzed in this paper. All conditions were presented in random order, separated by short breaks. Videos were shown on a back-projection screen (videos were 41 cm × 35 cm in size) placed in front of the participants at a distance of ~1 m. Sounds were delivered at 60 dB (measured at ear-level) through a front-facing speaker (Panphonics Oy, Espoo, Finland) placed ~1 m behind the screen. Participants were instructed to watch the videos and listen to the sounds attentively.

To investigate our research hypotheses, we focussed on the following conditions: 1) the original speech audio with no video, referred to as *audio-only*, 2) the original video with no audio, referred to as *video-only*, 3) the control video with no audio, referred to as the *control-video-only*, and 4) the *rest*.

Data acquisition

Neuromagnetic signals were acquired with a whole-scalp-covering neuromagnetometer (Vectorview; Elekta Oy, Helsinki, Finland) in a magnetically shielded room. The recording pass-band was 0.1–330 Hz and the signals were sampled at 1 kHz. The head position inside the MEG helmet was continuously monitored by feeding current to 4 head-tracking coils located on the scalp. Head position indicator coils, three anatomical fiducials, and at least 150 head-surface points (covering the whole scalp and the nose surface) were localized in a common coordinate system using an electromagnetic tracker (Fastrak, Polhemus, Colchester, VT, USA).

Eye movements were tracked with an MEG-compatible eye tracker (EyeLink 1000 Plus, SR Research). Participants were calibrated using the standard 9-point display and monocular eye movements were recorded at a sampling rate of 1 kHz. Eye-movements were recorded for the duration of all experimental conditions.

High-resolution 3D-T1 cerebral magnetic resonance images (MRI) were acquired on a 3 Tesla MRI scan (Siemens Medical System, Erlangen, Germany) facility available at the BCBL.

MEG preprocessing

Continuous MEG data were first preprocessed off-line using the temporal signal space separation method (correlation coefficient, 0.9; segment length, 10 s) to suppress external sources of interference and to correct for head movements (Taulu et al., 2005; Taulu and Simola, 2006). To further suppress heartbeat, eye-blink, and eye-movement artifacts, 30 independent components (Vigário et al., 2000; Hyvärinen et al., 2004) were evaluated from the MEG data low-pass filtered at 25 Hz using FastICA algorithm (dimension reduction, 30; non-linearity, tanh). Independent components corresponding to such artifacts were identified based on their topography and time course and were removed from the full-rank MEG signals.

Coherence analysis

Coherence was estimated between MEG signals and 1) the auditory speech temporal envelope, 2) mouth opening, 3) mouth width, and 4) mouth surface. The auditory speech temporal envelope was obtained by summing the Hilbert envelope of the auditory speech signal filtered through a third octave filter bank (central frequency ranging linearly on a log-scale from 250 Hz to 1600 Hz; 19 frequency bands), and was further resampled to 1000 Hz time-locked to the MEG signals (Fig. 1B). Continuous data from each condition were split into 2-s epochs with 1.6-s epoch overlaps, affording a spectral resolution of 0.5 Hz while decreasing noise on coherence estimates (Bortel and Sovka, 2014). MEG epochs exceeding 5 pT (magnetometers) or 1 pT/cm (gradiometers) were excluded from further analyses to avoid data contamination by artifact sources that had not been suppressed by the temporal signal

space separation or removed with independent component analysis. These steps led to an average of 732 artifact-free epochs across participants and conditions (SD = 36). A one-way repeated measures ANOVA revealed no differences between conditions ($F_{2,54}$ = 1.07, p = 0.35). Next, we estimated sensor-level coherence (Halliday, 1995) and combined gradiometer pairs based on the direction of maximum coherence (Bourguignon et al., 2015). Only values from these gradiometer pairs are presented in the results.

In coherence analyses, we focused on four frequency ranges (0.5 Hz, 1–3 Hz, 2–5 Hz, and 4–8 Hz) by averaging coherence across the frequency bins they encompassed. The 2–5-Hz, and 4–8-Hz frequency ranges were well matched to the count rate of words (3.34 ± 0.12 Hz; mean ± SD across the 8 videos) and syllables (5.91 ± 0.12 Hz), while the count rate of phrases (1.01 ± 0.20 Hz) fell in between the two lowest ranges. As in a previous study (Vander Ghinst et al., 2019), rates were assessed as the number of phrases, words, or syllables manually extracted from audio recordings divided by the corrected duration of the audio recording. For phrases, the corrected duration was trivially the total duration of the audio recording. For words and syllables, the corrected duration was the total time during which the talker was actually talking, that is the total duration of the audio recording (here 5 min) minus the sum of all silent periods when the auditory speech envelope was below a tenth of its mean for at least 100 ms. Note that setting the threshold for the duration defining a silent period to a value obviously too low (10 ms) or too high (500 ms) changed the estimates of word and syllable count rates by only ~10 %. These frequency ranges were selected also because auditory speech entrainment dominates at 0.5 Hz and 4–8 Hz (Luo and Poeppel, 2007; Bourguignon et al., 2012; Gross et al., 2013; Peelle et al., 2013; Molinaro et al., 2016; Vander Ghinst et al., 2016; Meyer et al., 2017; Meyer and Gumbert, 2018) but is also present at intermediate frequencies (Keitel et al., 2018), and because lip entrainment has

previously been identified at 2–5 Hz (Park et al., 2016; Giordano et al., 2017). Coherence maps were also averaged across participants for illustration purposes.

We only report coherence estimated between MEG signals and 1) the auditory speech envelope and 2) mouth opening. Although tightly related, the two latter signals displayed only a moderate degree of coupling, that peaked at 0.5 Hz, and 4–8 Hz (Fig. $2A_i$), with a visual–to–auditory speech delay of ~120-ms (maximum cross-correlation between auditory speech envelope and mouth opening; Fig. $2B_i$). Mouth opening and mouth surface were coherent at > 0.7 across the 0–10-Hz range (Fig. $2A_{ii}$) and yielded similar results. Mouth width displayed a moderate level of coherence with mouth opening (Fig. $2A_{iii}$) and an unclear visual–to–auditory speech delay (Fig. $2B_{ii}$). Mouth width was not included in the main analyses because it led to lower coherence values with MEG signals than mouth opening, but was retained as a nuisance factor in the partial coherence analyses (see below).

It is worth noting that the magnitude of the coupling between the auditory speech envelope and mouth opening (as assessed by coherence) we report for our audio-visual stimuli was 2–3 times lower than that reported elsewhere (Park et al., 2016; Hauswald et al., 2018). To ensure that this discrepancy was not due to the inadequacy of our lip-extraction procedure, we compared our time-series of mouth parameters to those extracted using a deep-learning-based solution (Visage Technology; face tracking and analysis). This revealed a good correspondence between the estimated time-series for mouth opening ($r = 0.95 \pm 0.01$; mean ± SD across the 8 videos), mouth width ($r = 0.88 \pm 0.01$), and mouth surface ($r = 0.95 \pm 0.01$). The genuine difference between the level of audio-visual speech coupling found in our study compared to others might be due to the language used (Spanish here vs. English elsewhere), or to the idiosyncrasies of our talker. Nevertheless, this relative decoupling between audio- and visual speech signals provided an opportunity to separate their respective cortical representations more efficiently.

Coherence was also estimated at the source level. To do so, individual MRIs were first segmented using the Freesurfer software (Reuter et al., 2012; RRID:SCR_001847). Then, the MEG forward model was computed using the Boundary Element Method implemented in the MNE software suite (Gramfort et al., 2014; RRID:SCR_005972) for three orthogonal tangential current dipoles (corresponding to the 3 spatial dimensions) placed on a homogeneous 5-mm grid source space covering the whole brain. At each source, the forward model was further reduced to its two first principal components, which closely corresponded to sources tangential to the skull; the discarded component corresponded to the radial source which is close to magnetically silent. Coherence maps were produced within the computed source space at 0.5 Hz, 1–3 Hz, 2–5 Hz, and 4–8 Hz using a linearly constrained minimum variance beamformer built based on the *rest* data covariance matrix (Van Veen et al., 1997; Hillebrand and Barnes, 2005). Source maps were then interpolated to a 1-mm homogenous grid and smoothed with a Gaussian kernel of 5 mm full-width-at-half-maximum. Both planar gradiometers and magnetometers were used for inverse modeling after dividing each sensor signal (and the corresponding forward-model coefficients) by the standard deviation of its noise. The noise variance was estimated from the continuous *rest* MEG data band-passed through 1–195 Hz, for each sensor separately.

Coherence maps were also produced at the group level. A non-linear transformation from individual MRIs to the MNI brain was first computed using the spatial normalization algorithm implemented in Statistical Parametric Mapping (SPM8; Ashburner et al., 1997; Ashburner and Friston, 1999; RRID:SCR_007037) and then applied to individual MRIs and coherence maps. This procedure generated a normalized coherence map in the MNI space for each subject and frequency range. Coherence maps were then averaged across participants.

Individual and group-level coherence maps for the auditory speech envelope (mouth opening, respectively) were also estimated after controlling for mouth opening and mouth

width (the auditory speech envelope, respectively) using partial coherence (Halliday, 1995). Partial coherence is the direct generalization of partial correlation (Kendall and Stuart, 1968) to the frequency domain (Halliday, 1995).

The same approach was used to estimate coherence between MEG (in the sensor and source space) and global changes (or edges) in the visual stimulus, and to partial out such "global visual change" from coherence maps for the auditory speech envelope. The global visual change signal was computed at every video frame as the sum of squares of the difference between that frame and the previous frame, divided by the sum of squares of the previous frame. This signal predominantly identified edges corresponding to periods when the speaker moved her head, eyebrows and jaw (see Fig. 3). The rationale being that these periods may tend to co-occur with the onset of phrases and sentences (Munhall et al., 2004) and could modulate oscillatory activity in auditory cortices (Schroeder et al., 2008).

Finally, individual and group-level coherence maps for the auditory speech envelope in *video-only* were estimated after shifting the auditory speech envelope by ~30 s, ~60 s, … ~240 s, and ~270 s. For each subject and time-shift, the exact time-shift applied was selected within a ±10 s window around the target time-shift, at the silent period for which the auditory speech envelope smoothed with a 1-s square kernel was at the minimum. Ensuing values of coherence were used to rule out the possibility that coherence with the genuine auditory speech envelope results from general temporal characteristics of auditory speech.

Estimation of temporal response functions

We used temporal response functions (TRFs) to model how the auditory speech envelope affected the temporal dynamics of auditory cortical activity. Based on our results, TRFs were estimated only for the 0.2–1.5-Hz frequency range, in the *audio-only* and *video-only* conditions. A similar approach has been used to model brain responses to speech at 1–8 Hz (Lalor and Foxe, 2010; Zion Golumbic et al., 2013), and to model brain responses to

natural force fluctuations occurring during maintenance of constant hand grip contraction (Bourguignon et al., 2017b). TRFs are the direct analogue of evoked responses in the context of continuous stimulation.

We used the mTRF toolbox (Crosse et al., 2016) to estimate the TRF of auditory cortical activity associated with the auditory speech envelope. In all conditions, source signals were reconstructed at individual coordinates of maximum 0.5-Hz coherence with the auditory speech envelope in *audio-only*. These two-dimensional source signals were projected onto the orientation that maximized the coherence with the auditory speech envelope at 0.5 Hz. Then, the source signal was filtered at 0.2–1.5 Hz, the auditory speech envelope was convolved with a 50-ms square smoothing kernel and both were down-sampled to 20 Hz (note that for auditory speech envelope, this procedure is equivalent to taking the mean over samples 25 ms around sampling points). For each subject, the TRFs were modeled from –1.5 s to +2.5 s, for a fixed set of ridge values ($\lambda = 2^0, 2^1, 2^2 \ldots 2^{20}$). We adopted the following 10-fold cross-validation procedure to determine the optimal ridge value: For each subject, TRFs were estimated based on 90% of the data, and used to predict the 10% of data left out and the Pearson correlation was then estimated between predicted and measured signals. The square of the mean correlation value across the 10 runs provided an estimate of the proportion of variance explained by entrainment to the auditory speech envelope. TRFs were recomputed based on all the available data for the ridge value maximizing the mean explained variance. To deal with sign ambiguity, the polarity of each TRF was adapted so that correlation with the first singular vector of all subjects' TRF in the range –0.5 s to 1.0 s is positive.

Based on our results, the TRF framework was also used to model brain responses to mouth opening and the global visual change signal at 0.2–1.5 Hz and mouth opening at 2–5 Hz, and to model the evolution of the auditory speech envelope at 0.2–1.5 Hz associated with

the time course of (i) mouth opening, (ii) global visual change, and (iii) the Hilbert envelope of mouth opening in the 2–5-Hz band. Note that the last TRF seeks phase–amplitude coupling between auditory speech envelope at 0.2–1.5 Hz (phase) and mouth opening at 2–5 Hz (amplitude), with the—perhaps not that common—perspective that the amplitude signal drives the phase signal. We used exactly the same parameters as reported above, except the data for the brain response to mouth opening at 2–5 Hz where were downsampled to 50 Hz and modeled from –0.7 to 1.2 s.

Eye-tracking data

As in previous studies using eye-tracking (McMurray et al., 2002; Kapnoula et al., 2015), eye-movements were automatically parsed into saccades and fixations using default psychophysical parameters. Adjacent saccades and fixations were combined into a single "look" that started at the onset of the saccade and ended at the offset of the fixation.

A region of interest was identified for each of the three critical objects: mouth and eyes in *video-only* and flickering cross in *control-video-only* (Fig. 4). In converting the coordinates of each look to the object being fixated, the boundaries of the regions of interest were extended by 50 pixels in order to account for noise and/or head-drift in the eye-tracking record. This did not result in any overlap between the eye and mouth regions.

Based on these regions of interest, we estimated the proportion of eye fixation to the combined regions of interest encompassing eyes and mouth in *video-only* and flickering cross in *control-video-only*. Eyes and mouth regions were combined because these are the parts of the face people tend to look at when watching a talking face (Vatikiotis-Bateson et al., 1998). Importantly, even when people are looking at the eyes, lip movements—in the periphery of the field of view—still benefit speech perception (Paré et al., 2003; Kaplan and Jesse, 2019). The two resulting areas were of comparable size: 100,800 pixels for the flickering cross vs. 77,300 pixels for the eyes and mouth. Data from one participant were excluded due to

technical issues during acquisition, and eye fixation analyses were thus based on data from 27 participants.

Experimental design and statistical analyses

Sample size was based on previous studies reporting entrainment to lip movements, which included 46 (Park et al., 2016) and 19 (Giordano et al., 2017) healthy adults.

The statistical significance of the local coherence maxima observed in group-level maps was assessed with a non-parametric permutation test that intrinsically corrects for multiple spatial comparisons (Nichols and Holmes, 2002). Subject- and group-level *rest* coherence maps were computed in a similar way to the *genuine* maps; MEG signals were replaced by *rest* MEG signals while auditory/visual speech signals were identical. Group-level difference maps were obtained by subtracting *genuine* and *rest* group-level coherence maps. Under the null hypothesis that coherence maps are the same irrespective of the experimental condition, *genuine* and *rest* labels should be exchangeable at the subject-level prior to computing the group-level difference map (Nichols and Holmes, 2002). To reject this hypothesis and to compute a threshold of statistical significance for the correctly labeled difference map, the permutation distribution of the maximum of the difference map's absolute value was computed for a subset of 1000 permutations. The threshold at $p < 0.05$ was computed as the 95^{th} percentile of the permutation distribution (Nichols and Holmes, 2002). Permutation tests can be too conservative for voxels other than the one with the maximum observed statistic (Nichols and Holmes, 2002). For example, dominant coherence values in the right auditory cortex could bias the permutation distribution and overshadow weaker coherence values in the left auditory cortex, even if these were highly consistent across subjects. Therefore, the permutation test described above was conducted separately for left- and right-hemisphere voxels. All supra-threshold local coherence maxima were

interpreted as indicative of brain regions showing statistically significant coupling with the auditory or visual signal.

A confidence volume was estimated for all significant local maxima, using the bootstrap-based method described in Bourguignon et al. (2017a). The location of the maxima was also compared between conditions using the same bootstrap framework (Bourguignon et al., 2017a).

For each local maximum, individual maximum coherence values were extracted within a 10-mm sphere centered on the group level coordinates, or on the coordinates of maxima for *audio-only*. Coherence values were compared between conditions or signals of reference with two-sided paired *t*-tests.

The bootstrap method was used to assess the timing of peak TRFs (Efron and Tibshirani, 1993). As a preliminary step, TRFs were upsampled by spline interpolation to 1000 Hz. A bootstrap distribution based on 10000 random drawings of subjects (or videos) was then built for the timing of peak TFR, from which we extracted the mean and standard deviation. Also the bias-corrected and accelerated bootstrap (Efron and Tibshirani, 1993) was used to compare the timing of peak TRF between conditions.

For the eye-tracking data, individual proportions of fixations were transformed using the empirical-logit transformation (Collins et al., 1992). Fixations to eyes and mouth in *video-only* were compared to fixations to the flickering cross in *control-video-only* using a two-sided paired *t*-test across participants.

Data and software availability

MEG and eye-tracking data as well as video stimuli are available on request from the corresponding author.

Results

Table 1 provides the coordinates and significance level of the loci of statistically significant coherence with the auditory speech envelope (henceforth, speech entrainment) and mouth opening (henceforth, lip entrainment) in all conditions (*audio-only*, *video-only*, and *control-video-only*) at all the selected frequency ranges (0.5 Hz, 1–3 Hz, 2–5 Hz, and 4–8 Hz).

Entrainment to heard speech

In *audio-only,* significant speech entrainment peaked at sensors covering bilateral auditory regions in all the explored frequency ranges: 0.5-Hz (Fig. 5A), 1–3 Hz (Fig. 6A), 2–5 Hz (Fig. 6B), and 4–8 Hz (Fig. 6C). Underlying sources were located in bilateral auditory cortices (Fig. 5A, 6, and Table 1).

Auditory cortices entrain to absent speech at frequencies below 1 Hz

In *visual-only*, there was significant 0.5-Hz entrainment to the speech sound that was actually produced by the speaker, but not heard by participants (see Fig. 5B and Table 1). The significant loci for speech entrainment were the bilateral auditory cortices, the left inferior frontal gyrus, and the inferior part of the left precentral sulcus (Fig. 5B and Table 1). Critically, the location of the auditory sources where we observed maximum 0.5-Hz entrainment did not differ significantly between *audio-only* and *video-only* (left, $F_{3,998} = 1.62$, $p = 0.18$; right, $F_{3,998} = 0.85$, $p = 0.47$). Not surprisingly, the magnitude of 0.5-Hz speech entrainment was higher in *audio-only* than in *video-only* (left, $t_{27} = 6.36$, $p < 0.0001$; right, $t_{27} = 6.07$, $p < 0.0001$). Nevertheless, brain responses associated with speech entrainment at ~0.5 Hz displayed a similar time-course in *audio-only* and *video-only* (see Fig. 5A and 5B). In the left hemisphere, brain response peaked after the auditory speech envelope with a delay that did not differ significantly between the two conditions (*audio-only*, 18 ± 19 ms, *video-only*,

73 ± 47 ms; $p = 0.27$); in the right hemisphere this delay was significantly shorter for *audio-only* (43 ± 38 ms) than *video-only* (216 ± 54 ms; $p = 0.019$). These results demonstrate that within the auditory cortices, neuronal activity at ~0.5 Hz is modulated similarly by heard speech sounds and absent speech when lip-read information is available, but incurs an additional delay in the right hemisphere. Next, we address four critical questions related to this effect: 1) Can it be explained by the general temporal characteristics of auditory speech? 2) Is it unspecific to seeing the speaker's face? 3) Is it a direct result of lip-reading induced visual activity simply being fed to auditory areas? 4) Is it mediated by edges in the visual stimuli (predominantly reflecting head, eyebrows and jaw movements) that would prime phrase/sentence onset and modulate auditory cortical activity. A negative answer to these 4 questions would support the view that auditory speech envelope is "synthesized" through internal models that map visual speech onto sound features.

Below 1-Hz entrainment to absent speech is not explained by the general temporal characteristics of auditory speech

In *video-only*, auditory sources (coordinates identified in *audio-only*) entrained significantly more to the corresponding—though absent—auditory speech than to unrelated auditory speech, here taken as the corresponding speech shifted in time (left, $t_{27} = 3.08$, $p = 0.0047$; right, $t_{27} = 3.78$, $p = 0.0008$; see Fig. 7A). In this analysis, individual subject values were computed as the mean value across all considered time shifts. In addition, inspection of the maps of entrainment to unrelated speech did not reveal any special tendency to peak in auditory regions. This demonstrates that entrainment to absent speech in auditory cortices is not a consequence of the general temporal characteristics of auditory speech.

Below 1 Hz entrainment to absent speech is specific to seeing speaker's face

Analysis of a *control-visual-only* condition revealed that entrainment to unheard speech at auditory cortices was specific to seeing the speaker's face. In the control condition, participants were looking at a silent video of a flickering Greek cross whose luminance pattern dynamically encoded the speaker's mouth configuration. We observed luminance-driven entrainment at 0.5 Hz at occipital cortices (Table 1), but no significant entrainment with unheard speech ($p > 0.1$, Fig. 7B). Importantly, speech entrainment at auditory sources (coordinates identified in *audio-only*) was significantly higher in *video-only* than in *control-video-only* (left, $t_{27} = 3.44$, $p = 0.0019$; right, $t_{27} = 4.44$, $p = 0.00014$, see Fig. 7A). These differences in auditory speech entrainment cannot be explained by differences in attention as participants attended the flickering cross in *control-video-only* approximately as much as speaker's eyes and mouth in *video-only* (81.0 ± 20.9% vs. 87.5 ± 17.1%; $t_{26} = 1.30$, $p = 0.20$: fixation data derived from eye-tracking recordings). This demonstrates that auditory cortical entrainment to unheard speech is specific to seeing the speaker's face.

Below 1-Hz entrainment to absent speech does not result from a direct feeding of lip movements to auditory cortices

Although driven by lip-read information, auditory cortical activity at ~0.5 Hz in *visual-only* entrained more to unheard speech than to seen lip movements. Indeed, speech entrainment was stronger than lip entrainment at the left auditory source coordinates identified in *audio-only* ($t_{27} = 2.52$, $p = 0.018$, see Fig. 7A). The same trend was observed at the right auditory source ($t_{27} = 1.98$, $p = 0.058$, see Fig. 7A). However, at 0.5 Hz, lip movements entrained brain activity in the right angular gyrus (Fig. 7C and Table 1), a visual integration hub implicated in biological motion perception (Allison et al., 2000; Puce and Perrett, 2003). Such entrainment entailed a visual-speech-to-brain delay of 40 ± 127 ms. Note

494 that the dominant source of lip and speech entrainment were ~4 cm apart ($F_{3,998}$ = 4.68, p =
495 0.0030). Still, despite being distinct, their relative proximity might be the reason why speech
496 entrainment was only marginally higher than lip entrainment in the right auditory cortex.
497 Indeed, due to issues inherent to reconstructing brain signals based on extracranial signals
498 (known as source leakage), lip entrainment estimated at the auditory cortex was artificially
499 enhanced by the source in the angular gyrus. This leads us to conclude that entrainment in
500 bilateral auditory cortices occurred with unheard speech rather than with seen lip movements.
501 As further support for this claim, speech entrainment was still significant bilaterally in
502 auditory cortices after partialling out lip movements (mouth opening and width; see Fig. 7D).
503 In the right hemisphere, it peaked 2.2 mm away from sources observed without partialling out
504 lip movements. In the left hemisphere, the peak in the partial coherence map was displaced
505 towards the middle temporal gyrus (MNI coordinates: [–64 –21 –9]). Although it did not
506 peak in the left auditory cortex, the source distribution of the partial coherence was clearly
507 pulled towards that brain region.

508 ***Below 1-Hz entrainment to absent speech is not explained by modulation of auditory***
509 ***activity by edges in the visual stimulus***

510 Speech entrainment did not differ significantly from entrainment to the global visual
511 change signal at the coordinates of bilateral auditory sources identified in *audio-only* (left, t_{27}
512 = 1.17, p = 0.25; right, t_{27} = 1.10, p = 0.28, see Fig. 7A). However, entrainment to the global
513 visual change signal at ~0.5 Hz was significant only in the posterior part of the right superior
514 temporal gyrus (MNI coordinates: [62 –32 21]), with a visual-change-to-brain delay of 149 ±
515 33 ms (See Fig. 7E). Most importantly, speech entrainment corrected for the global visual
516 change signal still peaked and was significant in three left hemisphere sources that were less
517 than 2.5 mm away from those of uncorrected speech entrainment (see Fig. 7F). Corrected
518 speech entrainment in the right hemisphere peaked 1 mm away from the right auditory source

519 of uncorrected speech entrainment and was only marginally significant (p = 0.085). In sum,
520 global changes in the visual stimulus modulated oscillatory brain activity at ~0.5 Hz in the
521 right posterior superior temporal gyrus, but such modulation did not mediate the entrainment
522 to absent speech.

523 Altogether, our results support the view that auditory speech envelope is synthesized
524 through lip-reading.

525 ***Entrainment to absent speech at other frequencies***

526 At 1–3 Hz, there was significant entrainment to the absent speech in *visual-only* but
527 not in *control-visual-only* (see Table 1). Significant entrainment to absent speech in *visual-*
528 *only* peaked in the posterior part of the left inferior temporal gyrus, and in the central part of
529 the middle temporal gyrus (see Table 1).

530 Entrainment in the posterior part of the left inferior temporal gyrus was specific to
531 seeing the speaker's face (comparison *visual-only* vs. *control-visual-only*: t_{27} = 2.72, p =
532 0.011) but did not entail a synthesis process since speech entrainment at this location was not
533 significantly different from lip entrainment (t_{27} = 1.30, p = 0.20). It did not reach significance
534 after partialling out mouth movements (see Table 1).

535 Entrainment in the central part of the middle temporal gyrus was not specific to seeing
536 the speaker's face (comparison *visual-only* vs. *control-visual-only*: t_{27} = 1.48, p = 0.15) and
537 did not entail a synthesis process since speech entrainment at this location was not
538 significantly different from lip entrainment (t_{27} = –0.10, p = 0.92) despite surviving
539 partialling out of mouth movements.

540 At 2–5 Hz, there was no significant entrainment to the absent speech in *visual-only*
541 nor in *control-visual-only*.

At 4–8 Hz, there was significant entrainment to the absent speech in *video-only* and *control-video-only*, but only in occipital areas, and it vanished after partialling out the contribution of lip movements.

Entrainment to lip movements

Lip entrainment at 1–3 Hz, 2–5 Hz, and 4–8 Hz trivially occured in occipital cortices in *video-only* and *control-video-only* (Table 1). Figure 8 illustrates entrainment at 2–5 Hz which we had planned to focus on based on previous reports (Park et al., 2016; Giordano et al., 2017). Brain responses associated with lip entrainment at 2–5 Hz peaked with a delay of 115 ± 8 ms (first source) and 159 ± 8 ms (second source).

Our data do not suggest the presence of entrainment to unseen lip movements in visual cortices in *audio-only*. Indeed, in that condition, significant lip entrainment at 0.5 Hz occurred only in auditory cortices, and disappeared when we partialled out entrainment to the auditory speech envelope. No significant lip entrainment in this condition was found at any of the other tested frequency ranges: 1–3 Hz, 2–5 Hz and 4–8 Hz.

Delays between auditory and visual speech

Time-efficient synthesis of the auditory speech envelope might rely on the visual-to-auditory lag inherent to natural speech. Indeed, in our audio-visual stimuli, the ~0.5-Hz auditory speech envelope peaked 87 ± 9 ms after the ~0.5-Hz mouth-opening time-course (see Fig. 9 left). But our results indicate that in *visual-only*, visual activity entrains to 2–5-Hz mouth movements while auditory activity entrains to an ~0.5-Hz absent auditory speech envelope. The simplest way to connect these oscillations is through phase–amplitude coupling, whereby the amplitude of 2–5-Hz visual activity modulates the phase of ~0.5-Hz auditory activity. Accordingly, we also estimated the delay from the envelope of 2–5-Hz

565 mouth opening time-course to ~0.5-Hz auditory speech envelope, and found it was 170 ± 7
566 ms (see Fig. 9 middle).

567 Also important is the interplay between global changes in the visual stimulus (mainly
568 driven by head, eyebrows and jaw movements) and auditory speech envelope. This is because
569 global visual changes could in principle modulate auditory cortical activity and hence
570 mediate entrainment to absent speech. And indeed, in our audio-visual stimuli, the ~0.5-Hz
571 auditory speech envelope peaked 73 ± 22 ms after the ~0.5-Hz global visual change signal
572 (see Fig. 9 right), meaning that low-level visual changes can cue slow changes in speech
573 envelope (indicating phrase/sentence boundaries). However, the global visual change signal
574 and the auditory speech envelope were only weakly coupled at ~0.5 Hz (mean ± SD
575 coherence across the 8 video stimuli: 0.051 ± 0.022) and in the other frequency ranges we
576 explored. For a comparison, this degree of coupling was significantly lower than that between
577 mouth opening and the auditory speech envelope ($t_7 = 5.63$, $p = 0.0008$; paired t-test on the
578 coherence values for the 8 videos). In other words, lip movements provide more information
579 about speech envelope than global changes in the visual stimulus, and similar temporal lead
580 on auditory speech envelope (see Fig. 9). This further supports the view that auditory cortical
581 entrainment to silent speech results from a fast synthesis process driven by lip reading rather
582 than from modulation of auditory activity driven by the identification of low-level cross-
583 sensory correspondences.

584

585 **Discussion**

586 We have demonstrated that the brain synthesises the slow (below 1 Hz) temporal
587 dynamics of unheard speech from lip-reading. Specifically, watching silent lip-read videos
588 without prior knowledge of what the speaker is saying leaves a trace of the auditory speech
589 envelope in auditory cortices that closely resembles that left by the actual speech sound.

590

591 ***Entrainment to unheard speech in auditory cortices***

592 Our most striking finding was that lip-reading induced entrainment in auditory
593 cortices to the absent auditory speech at frequencies below 1 Hz. This entrainment 1) was
594 specific to lip-reading, 2) was not a consequence of the general temporal characteristics of
595 auditory speech, 3) was not a mere byproduct of entrainment to lip movements, and 4) was
596 not mediated by low-level changes in the visual stimulus (at least in the left hemisphere).
597 Instead, this genuine entrainment is similar to the entrainment induced by actual auditory
598 speech: both are rooted in bilateral auditory cortices and are characterized by similar time-
599 courses, though with an additional delay of ~200 ms in the right hemisphere. This suggests
600 the existence of a time-efficient synthesis mechanism that maps facial articulatory mouth
601 gestures onto corresponding speech sound features. Such a mechanism would likely leverage
602 the natural visual–to–auditory speech delay (90–170 ms) and could be explained by visually-
603 driven predictive coding (Friston and Kiebel, 2009). Likewise, auditory-driven predictive
604 coding could account for the short (below-50-ms) latencies observed here in *audio-only* (Park
605 et al., 2015).

606 Importantly, such auditory entrainment is unlikely to be driven by auditory imagery.
607 Auditory imagery reflects perceptual auditory processing not triggered by external auditory
608 stimulation (Nanay, 2018). In principle, observation of lip movements could lead to auditory
609 imagery of related or unrelated speech or non-speech sounds. Clearly, auditory imagery of
610 the actual speech sounds was never an option since participants were not professional lip-
611 readers and were not cued about speech content. Furthermore, our results demonstrate that
612 the auditory entrainment we observed cannot be linked to auditory imagery of unrelated
613 sounds either since it was stronger for the corresponding but absent sound than for either seen

lip movements or unrelated speech. Accordingly, the fast synthesis hypothesis we have suggested seems to be the most likely interpretation of the observed entrainment.

The synthesis mechanism we have uncovered is likely grounded in the fact that lip-read information is coupled to the auditory signal in space and time (Munhall and Vatikiotis-Bateson, 2004; Chandrasekaran et al., 2009). In addition, the phonetic identity of each phoneme is supported by sound as well by the configuration of the lips. Even young infants are sensitive to this type of correspondence (Kuhl and Meltzoff, 1982), and phonetic integration continues to develop into adulthood, where the first traces of speech-specific phonetic integration are observed within ~250 ms after sound onset (Stekelenburg and Vroomen, 2012; Baart et al., 2014). Presumably, the tight audiovisual coupling in speech lies at the foundation of lip-read-induced entrainment to absent auditory speech in the brain, and there is indeed much evidence for entrainment to auditory speech at phrase and syllable rates (Luo and Poeppel, 2007; Bourguignon et al., 2012; Gross et al., 2013; Peelle et al., 2013; Molinaro et al., 2016; Vander Ghinst et al., 2016; Meyer et al., 2017; Meyer and Gumbert, 2018).

Frequencies below 1 Hz match with phrasal, stress and sentential rhythmicity. Accordingly, corresponding entrainment to heard speech sounds has been hypothesised to subserve parsing or chunking of phrases and sentences (Ding et al., 2016; Meyer et al., 2017), or to help align neural excitability with syntactic information to optimize language comprehension (Meyer and Gumbert, 2018). Hence, our data suggest that such entrainment/alignment can be obtained through lip-reading, thereby facilitating speech chunking, parsing, and extraction of syntactic information.

As 4–8 Hz frequencies match with syllable rate, corresponding entrainment has been hypothesised to reflect parsing or chunking of syllables. Supporting this view, 4–8-Hz entrainment is enhanced when listening to intelligible speech compared to non-intelligible

639 speech (Ahissar et al., 2001; Luo and Poeppel, 2007; Peelle et al., 2013). However, we did
640 not observe such entrainment during silent lip-reading, which may suggest that the brain does
641 not synthesise the detailed phonology of unfamiliar silent syllabic structures based on lip-read
642 information only. After all, lip-reading is a very difficult task, even for professional lip-
643 readers (Chung et al., 2017). This is because different phonemes correspond to very similar
644 lip configurations (*e.g.*, /ba/, /pa/ and /ma/). However, when the auditory signal is known, this
645 ambiguity in the mapping between lip-reading and the corresponding phonemes disappears.
646 Indeed, it has been suggested that lip-reading can induce entrainment in auditory cortices at
647 frequencies above 1 Hz when participants are aware of the content of the visual-only speech
648 stimuli (Crosse et al., 2015).
649

650 ***Entrainment to lip movements***

651 During silent lip-reading, activity in early visual cortices entrained to lip movements
652 mainly at frequencies above 1 Hz, in line with previous studies (Park et al., 2016; Giordano et
653 al., 2017). Such occipital lip entrainment was reported to be modulated by audio-visual
654 congruence (Park et al., 2016). This is probably the first necessary step for the brain to
655 synthesize features of the absent auditory speech. Our results suggest that corresponding
656 signals are forwarded to the right angular gyrus (Hauswald et al., 2018).

657 The right angular gyrus was the dominant source of lip entrainment at frequencies
658 below 1 Hz. It is the convergence area for the dorsal and ventral visual streams and is
659 specialised for processing visual biological motion (Perrett et al., 1989; Allison et al., 2000;
660 Puce and Perrett, 2003; Marty et al., 2015). The right angular gyrus—or more precisely an
661 area close to it termed the temporal visual speech area (Bernstein et al., 2011; Bernstein and
662 Liebenthal, 2014)—activates during lip-reading (Calvert et al., 1997; Allison et al., 2000;
663 Campbell et al., 2001) and observation of mouth movements (Puce et al., 1998). It has also

been suggested that it maps visual input onto linguistic representation during reading (Démonet et al., 1992), and lipreading (Hauswald et al., 2018). Our results shed light on the oscillatory dynamics underpinning such mapping during lip-reading: based on visual input at dominant lip movement frequencies (above 1 Hz), the angular gyrus presumably extracts features of lip movements below 1 Hz, which can then serve as an intermediate step to synthesise speech sound features. Given the short lip-to-brain delay observed in this brain area (~40 ms), such extraction might rely on the prediction of mouth movements.

Entrainment to unheard speech in visual cortices

Previous studies that have examined the brain dynamics underlying lipreading of silent connected visual speech have essentially focused on visuo-phonological mapping in occipital cortices (O'Sullivan et al., 2016; Lazard and Giraud, 2017; Hauswald et al., 2018). For example, it was shown that occipital 0.3–15-Hz EEG signals are better predicted by a combination of motion changes, visual speech features and the unheard auditory speech envelope than by motion changes alone (O'Sullivan et al., 2016). Also, visual activity has been reported to entrain more to absent speech at 4–7 Hz when a video is played forward rather than backward (Hauswald et al., 2018). Importantly, this effect was not driven by entrainment to lip movements since lip entrainment was similar for videos played forwards and backwards. Instead, it came with increased top-down drive from left sensorimotor cortices to visual cortices, indicating that visuo-phonological mapping had already taken place in early visual cortices through top-down mechanisms (O'Sullivan et al., 2016; Hauswald et al., 2018). Our study complements these results by showing that auditory cortices also entrain to unheard speech, but at frequencies below 1 Hz, probably based on earlier processes taking place in the occipital regions and the right angular gyrus.

689 ***Limitations and future perspectives***

690 We did not collect behavioral data from our participants. Further studies should
691 clarify how the synthesis mechanism we have uncovered relates to individual lip-reading
692 abilities, or susceptibility to the McGurk effect.

693 It also remains to be clarified what features of speech are synthesised, and under
694 which circumstances auditory cortices can entrain to absent speech at higher frequencies
695 (especially 4–8-Hz).

696 Finally, it will be important to specify which features of the articulatory mouth
697 gestures lead to below-1-Hz auditory entrainment to absent speech. This would require visual
698 control conditions in which, for example, lip movements are shown in isolation, or replaced
699 by point-light stimuli.

700

701 ***Conclusion***

702 Our results demonstrate that the brain can quickly synthesize a representation of
703 coarse-grained auditory speech features in early auditory cortices and shed light on the
704 underlying oscillatory dynamics. Seeing lip movements first modulates neuronal activity in
705 early visual cortices at frequencies that match articulatory lip movements (above 1 Hz).
706 Based on this activity, the right angular gyrus, putatively the temporal visual speech area,
707 extracts and possibly predicts the slower features of lip movements. Finally, these slower lip
708 movement dynamics are mapped onto their corresponding speech sound features and this
709 information is fed to auditory cortices. Receiving this information likely facilitates speech
710 parsing, in line with the hypothesised role of entrainment to heard speech at frequencies
711 below 1 Hz.

712 **References**

713 Ahissar E, Nagarajan S, Ahissar M, Protopapas A, Mahncke H, Merzenich MM (2001)
714 Speech comprehension is correlated with temporal response patterns recorded from
715 auditory cortex. Proc Natl Acad Sci U S A 98:13367–13372.

716 Allison T, Puce A, McCarthy G (2000) Social perception from visual cues: role of the STS
717 region. Trends in Cognitive Sciences 4:267–278 .

718 Ashburner J, Friston KJ (1999) Nonlinear spatial normalization using basis functions. Hum
719 Brain Mapp 7:254–266.

720 Ashburner J, Neelin P, Collins DL, Evans A, Friston K (1997) Incorporating prior knowledge
721 into image registration. Neuroimage 6:344–352.

722 Baart M, Stekelenburg JJ, Vroomen J (2014) Electrophysiological evidence for speech-
723 specific audiovisual integration. Neuropsychologia 53:115–121.

724 Bernstein LE, Auer ET, Moore JK, Ponton CW, Don M, Singh M (2002) Visual speech
725 perception without primary auditory cortex activation. Neuroreport 13:311–315.

726 Bernstein LE, Jiang J, Pantazis D, Lu Z-L, Joshi A (2011) Visual phonetic processing
727 localized using speech and nonspeech face gestures in video and point-light displays.
728 Human Brain Mapping 32:1660–1676.

729 Bernstein LE, Liebenthal E (2014) Neural pathways for visual speech perception. Front
730 Neurosci 1:386.

731 Bortel R, Sovka P (2014) Approximation of the null distribution of the multiple coherence
732 estimated with segment overlapping. Signal Processing 96:310–314.

733 Bourguignon M, De Tiège X, Op de Beeck M, Ligot N, Paquier P, Van Bogaert P, Goldman
734 S, Hari R, Jousmäki V (2012) The pace of prosodic phrasing couples the listener's
735 cortex to the reader's voice. Hum Brain Mapp 34:314–326.

736 Bourguignon M, Molinaro N, Wens V (2017a) Contrasting functional imaging parametric

maps: The mislocation problem and alternative solutions. Neuroimage 169:200–211.

Bourguignon M, Piitulainen H, De Tiège X, Jousmäki V, Hari R (2015) Corticokinematic coherence mainly reflects movement-induced proprioceptive feedback. Neuroimage 106:382–390.

Bourguignon M, Piitulainen H, Smeds E, Zhou G, Jousmäki V, Hari R (2017b) MEG Insight into the Spectral Dynamics Underlying Steady Isometric Muscle Contraction. J Neurosci 37:10421–10437.

Calvert GA, Bullmore ET, Brammer MJ, Campbell R, Williams SC, McGuire PK, Woodruff PW, Iversen SD, David AS (1997) Activation of auditory cortex during silent lipreading. Science 276:593–596.

Campbell R, MacSweeney M, Surguladze S, Calvert G, McGuire P, Suckling J, Brammer MJ, David AS (2001) Cortical substrates for the perception of face actions: an fMRI study of the specificity of activation for seen speech and for meaningless lower-face acts (gurning). Brain Res Cogn Brain Res 12:233–243.

Chandrasekaran C, Trubanova A, Stillittano S, Caplier A, Ghazanfar AA (2009) The natural statistics of audiovisual speech. PLoS Comput Biol 5:e1000436.

Chung JS, Senior A, Vinyals O, Zisserman A (2017) Lip Reading Sentences in the Wild. In: 2017 IEEE Conference on Computer Vision and Pattern Recognition (CVPR).

Collins JJ, Fanciulli M, Hohlfeld RG, Finch DC, Sandri G v. H, Shtatland ES (1992) A random number generator based on the logit transform of the logistic variable. Computers in Physics 6:630.

Crosse MJ, Di Liberto GM, Bednar A, Lalor EC (2016) The Multivariate Temporal Response Function (mTRF) Toolbox: A MATLAB Toolbox for Relating Neural Signals to Continuous Stimuli. Front Hum Neurosci 10:604.

Crosse MJ, ElShafei HA, Foxe JJ, Lalor EC (2015) Investigating the temporal dynamics of

auditory cortical activation to silent lipreading. In: 2015 7th International IEEE/EMBS Conference on Neural Engineering (NER).

Démonet JF, Chollet F, Ramsay S, Cardebat D, Nespoulous JL, Wise R, Rascol A, Frackowiak R (1992) The anatomy of phonological and semantic processing in normal subjects. Brain 115:1753–1768.

Ding N, Melloni L, Zhang H, Tian X, Poeppel D (2016) Cortical tracking of hierarchical linguistic structures in connected speech. Nat Neurosci 19:158–164.

Efron B, Tibshirani RJ (1993) An Introduction to the Bootstrap.

Eveno N, Caplier A, Coulon P-Y (2004) Accurate and Quasi-Automatic Lip Tracking. IEEE Trans Circuits Syst Video Technol 14:706–715.

Friston K, Kiebel S (2009) Predictive coding under the free-energy principle. Philos Trans R Soc Lond B Biol Sci 364:1211–1221.

Giordano BL, Ince RAA, Gross J, Schyns PG, Panzeri S, Kayser C (2017) Contributions of local speech encoding and functional connectivity to audio-visual speech perception. Elife 6:e24763.

Gramfort A, Luessi M, Larson E, Engemann DA, Strohmeier D, Brodbeck C, Parkkonen L, Hämäläinen MS (2014) MNE software for processing MEG and EEG data. Neuroimage 86:446–460.

Gross J, Hoogenboom N, Thut G, Schyns P, Panzeri S, Belin P, Garrod S (2013) Speech rhythms and multiplexed oscillatory sensory coding in the human brain. PLoS Biol 11:e1001752.

Halliday D (1995) A framework for the analysis of mixed time series/point process data—Theory and application to the study of physiological tremor, single motor unit discharges and electromyograms. Prog Biophys Mol Biol 64:237–278.

Hauswald A, Lithari C, Collignon O, Leonardelli E, Weisz N (2018) A Visual Cortical

787 Network for Deriving Phonological Information from Intelligible Lip Movements. Curr
788 Biol 28:1453–1459.e3.
789 Hillebrand A, Barnes GR (2005) Beamformer Analysis of MEG Data. International Review
790 of Neurobiology 68:149–171.
791 Hyvärinen A, Karhunen J, Oja E (2004) Independent Component Analysis. John Wiley &
792 Sons.
793 Kaplan E, Jesse A (2019) Fixating the eyes of a speaker provides sufficient visual
794 information to modulate early auditory processing. Biol Psychol 146:107724.
795 Kapnoula EC, Packard S, Gupta P, McMurray B (2015) Immediate lexical integration of
796 novel word forms. Cognition 134:85–99.
797 Keitel A, Gross J, Kayser C (2018) Perceptually relevant speech tracking in auditory and
798 motor cortex reflects distinct linguistic features. PLoS Biol 16:e2004473.
799 Kendall MG, Stuart A (1968) The Advanced Theory of Statistics. The Statistician 18:163.
800 Kuhl PK, Meltzoff AN (1982) The bimodal perception of speech in infancy. Science
801 218:1138–1141.
802 Lalor EC, Foxe JJ (2010) Neural responses to uninterrupted natural speech can be extracted
803 with precise temporal resolution. Eur J Neurosci 31:189–193.
804 Lazard DS, Giraud A-L (2017) Faster phonological processing and right occipito-temporal
805 coupling in deaf adults signal poor cochlear implant outcome. Nat Commun 8:14872.
806 Luo H, Poeppel D (2007) Phase patterns of neuronal responses reliably discriminate speech
807 in human auditory cortex. Neuron 54:1001–1010.
808 Marty B, Bourguignon M, Jousmäki V, Wens V, Op de Beeck M, Van Bogaert P, Goldman
809 S, Hari R, De Tiège X (2015) Cortical kinematic processing of executed and observed
810 goal-directed hand actions. Neuroimage 119:221–228.
811 McMurray B, Tanenhaus MK, Aslin RN (2002) Gradient effects of within-category phonetic

variation on lexical access. Cognition 86:B33–42.

Meyer L, Gumbert M (2018) Synchronization of Electrophysiological Responses with Speech Benefits Syntactic Information Processing. J Cogn Neurosci:1–10.

Meyer L, Henry MJ, Gaston P, Schmuck N, Friederici AD (2017) Linguistic Bias Modulates Interpretation of Speech via Neural Delta-Band Oscillations. Cereb Cortex 27:4293–4302.

Molinaro N, Lizarazu M, Lallier M, Bourguignon M, Carreiras M (2016) Out-of-synchrony speech entrainment in developmental dyslexia. Hum Brain Mapp 37:2767–2783.

Munhall KG, Jones JA, Callan DE, Kuratate T, Vatikiotis-Bateson E (2004) Visual prosody and speech intelligibility: head movement improves auditory speech perception. Psychol Sci 15:133–137.

Munhall KG, Vatikiotis-Bateson E (2004) Spatial and Temporal Constraints on Audiovisual Speech Perception. In: The handbook of multisensory processes (Calvert GA, Spence C, Stein BE, eds), pp 177–188. Cambridge, MA, US: MIT Press.

Nanay B (2018) Multimodal mental imagery. Cortex 105:125–134.

Nichols TE, Holmes AP (2002) Nonparametric permutation tests for functional neuroimaging: a primer with examples. Hum Brain Mapp 15:1–25.

O'Sullivan AE, Crosse MJ, Di Liberto GM, Lalor EC (2016) Visual Cortical Entrainment to Motion and Categorical Speech Features during Silent Lipreading. Front Hum Neurosci 10:679.

Paré M, Richler RC, ten Hove M, Munhall KG (2003) Gaze behavior in audiovisual speech perception: the influence of ocular fixations on the McGurk effect. Percept Psychophys 65:553–567.

Park H, Ince RAA, Schyns PG, Thut G, Gross J (2015) Frontal top-down signals increase coupling of auditory low-frequency oscillations to continuous speech in human

837 listeners. Curr Biol 25:1649–1653.
838 Park H, Kayser C, Thut G, Gross J (2016) Lip movements entrain the observers' low-
839 frequency brain oscillations to facilitate speech intelligibility. Elife 5:e14521.
840 Paulesu E, Perani D, Blasi V, Silani G, Borghese NA, De Giovanni U, Sensolo S, Fazio F
841 (2003) A functional-anatomical model for lipreading. J Neurophysiol 90:2005–2013.
842 Peelle JE, Gross J, Davis MH (2013) Phase-locked responses to speech in human auditory
843 cortex are enhanced during comprehension. Cereb Cortex 23:1378–1387.
844 Pekkola J, Ojanen V, Autti T, Jääskeläinen IP, Möttönen R, Tarkiainen A, Sams M (2005)
845 Primary auditory cortex activation by visual speech: an fMRI study at 3 T. Neuroreport
846 16:125–128.
847 Perrett DI, Harries MH, Bevan R, Thomas S, Benson PJ, Mistlin AJ, Chitty AJ, Hietanen JK,
848 Ortega JE (1989) Frameworks of analysis for the neural representation of animate
849 objects and actions. J Exp Biol 146:87–113.
850 Puce A, Allison T, Bentin S, Gore JC, McCarthy G (1998) Temporal cortex activation in
851 humans viewing eye and mouth movements. J Neurosci 18:2188–2199.
852 Puce A, Perrett D (2003) Electrophysiology and brain imaging of biological motion. Philos
853 Trans R Soc Lond B Biol Sci 358:435–445.
854 Reuter M, Schmansky NJ, Rosas HD, Fischl B (2012) Within-subject template estimation for
855 unbiased longitudinal image analysis. Neuroimage 61:1402–1418.
856 Schroeder CE, Lakatos P, Kajikawa Y, Partan S, Puce A (2008) Neuronal oscillations and
857 visual amplification of speech. Trends Cogn Sci 12:106–113.
858 Stekelenburg JJ, Vroomen J (2012) Electrophysiological evidence for a multisensory speech-
859 specific mode of perception. Neuropsychologia 50:1425–1431.
860 Sumby WH, Pollack I (1954) Visual Contribution to Speech Intelligibility in Noise. J Acoust
861 Soc Am 26:212–215.

862 Taulu S, Simola J (2006) Spatiotemporal signal space separation method for rejecting nearby
863 interference in MEG measurements. Phys Med Biol 51:1759–1768.
864 Taulu S, Simola J, Kajola M (2005) Applications of the signal space separation method.
865 IEEE Trans Signal Process 53:3359–3372.
866 Vander Ghinst M, Bourguignon M, Niesen M, Wens V, Hassid S, Choufani G, Jousmäki V,
867 Hari R, Goldman S, De Tiège X (2019) Cortical Tracking of Speech-in-Noise Develops
868 from Childhood to Adulthood. J Neurosci 39:2938–2950.
869 Vander Ghinst M, Ghinst MV, Bourguignon M, Op de Beeck M, Wens V, Marty B, Hassid
870 S, Choufani G, Jousmäki V, Hari R, Van Bogaert P, Goldman S, De Tiège X (2016)
871 Left Superior Temporal Gyrus Is Coupled to Attended Speech in a Cocktail-Party
872 Auditory Scene. J Neurosci 36:1596–1606.
873 Van Veen BD, van Drongelen W, Yuchtman M, Suzuki A (1997) Localization of brain
874 electrical activity via linearly constrained minimum variance spatial filtering. IEEE
875 Trans Biomed Eng 44:867–880.
876 Vatikiotis-Bateson E, Eigsti I-M, Yano S, Munhall KG (1998) Eye movement of perceivers
877 during audiovisualspeech perception. Perception & Psychophysics 60:926–940.
878 Vigário R, Särelä J, Jousmäki V, Hämäläinen M, Oja E (2000) Independent component
879 approach to the analysis of EEG and MEG recordings. IEEE Trans Biomed Eng
880 47:589–593.
881 Zion Golumbic EM, Ding N, Bickel S, Lakatos P, Schevon CA, McKhann GM, Goodman
882 RR, Emerson R, Mehta AD, Simon JZ, Poeppel D, Schroeder CE (2013) Mechanisms
883 underlying selective neuronal tracking of attended speech at a “cocktail party.” Neuron
884 77:980–991.

885 **Figures and Tables:**

886

887 **Table 1**.

888 Significant peak of speech- and lip entrainment: peak MNI coordinates, significance level,
889 confidence volume, and anatomical location. Only significant peaks of speech-entrainment
890 that survived partialling out lip movements (exceptions marked with *) and global visual
891 changes (exceptions marked with **) are presented here. Likewise, only peaks of significant
892 lip entrainment that survived partialling out the auditory speech envelope are presented here.
893 For the exceptions, *ps* are displayed in between parentheses.

	Peak coordinates [mm]	*p*	Mean ± SD values	Confidence volume [cm^3]	Anatomical location
Speech entrainment at 0.5 Hz					
Audio-only	[–64 –19 8]	$<10^{-3}$	0.076 ± 0.045	2.6	Left auditory cortex
	[64 –21 6]	$<10^{-3}$	0.075 ± 0.046	5.5	Right auditory cortex
Video-only	[–46 –30 11]	0.003	0.025 ± 0.017	35.5	Left auditory cortex
	[68 –14 -2]**	0.029 (0.085)	0.024 ± 0.015	5.6	Right auditory cortex
	[–57 25 15]	0.005	0.021 ± 0.013	9.6	Left inferior frontal gyrus
	[–58 –15 41]*	0.018 (0.063)	0.023 ± 0.012	21.3	Left inferior precentral sulcus
Lip entrainment at 0.5 Hz					
Video-only	[49 –46 10]	0.002	0.022 ± 0.014	30.9	Right angular gyrus
Control-video-only	[10 –89 –21]	$<10^{-3}$	0.028 ± 0.023	6.3	Inferior occipital area
	[25 –96 –1]	0.008	0.027 ± 0.023	11.7	Right lateral occipital cortex
	[–23 –97 –4]	0.046	0.023 ± 0.014	39.1	Left lateral occipital cortex
Speech entrainment at 1–3 Hz					
Audio-only	[–62 –15 11]	$<10^{-3}$	0.031 ± 0.017	0.17	Lett auditory cortex
	[66 –10 9]	$<10^{-3}$	0.036 ± 0.022	0.22	Right auditory cortex
Video-only	[–51 –65 –16]	0.020	0.012 ± 0.004	58.8	Left inferior temporal gyrus
	[–67 –20 –12]*	0.005 (0.22)	0.012 ± 0.004	2.8	Left middle temporal gyrus
Lip entrainment at 1–3 Hz					
Video-only	[5 –92 –13]	$<10^{-3}$	0.015 ± 0.007	22.6	Calcarine cortex
	[33 –92 6]	0.001	0.014 ± 0.007	5.2	Right lateral occipital sulcus
	[–15 –96 12]	$<10^{-3}$	0.015 ± 0.005	18.3	Left calcarine cortex
Control-video-only	[1 –98 10]	$<10^{-3}$	0.029 ± 0.016	0.3	Calcarine cortex
	[34 –92 –3]	$<10^{-3}$	0.028 ± 0.016	0.9	Right lateral occipital cortex
	[–28 –94 –10]	$<10^{-3}$	0.023 ± 0.012	3.4	Left lateral occipital cortex
Speech entrainment at 2–5 Hz					
Audio-only	[67 –11 10]	$<10^{-3}$	0.020 ± 0.008	0.3	Left auditory cortex
	[–62 –14 13]	$<10^{-3}$	0.016 ± 0.007	0.4	Right auditory cortex
Lip entrainment at 2–5 Hz					
Video-only	[–14 –97 11]	$<10^{-3}$	0.018 ± 0.007	8.3	Left calcarine cortex
	[2 –93 –2]	$<10^{-3}$	0.018 ± 0.008	15.1	Calcarine cortex
Control-video-only	[–1 –98 11]	$<10^{-3}$	0.026 ± 0.016	1.8	Calcarine cortex
	[25 –97 –8]	$<10^{-3}$	0.025 ± 0.012	1.9	Right lateral occipital cortex
	[–28 –94 –10]	$<10^{-3}$	0.024 ± 0.012	0.3	Left lateral occipital cortex
Speech entrainment at 4–8 Hz					
Audio-only	[–64 –18 7]	$<10^{-3}$	0.013 ± 0.005	1.4	Left auditory cortex

	[67 –13 5]	$<10^{-3}$	0.020 ± 0.009	0.3	Right auditory cortex
Lip entrainment at 4–8 Hz					
Video-only	[10 –94 –4]	$<10^{-3}$	0.013 ± 0.005	19.3	Right calcarine cortex
	[–11 –95 9]	0.001	0.013 ± 0.004	18.8	Left calcarine cortex
Control-video-only	[–4 –88 –18]	$<10^{-3}$	0.016 ± 0.008	5.3	Inferior occipital cortex
	[27 –94 –5]	$<10^{-3}$	0.016 ± 0.007	22.5	Right lateral occipital cortex
	[–5 –97 15]	0.011	0.015 ± 0.006	30.0	Calcarine cortex

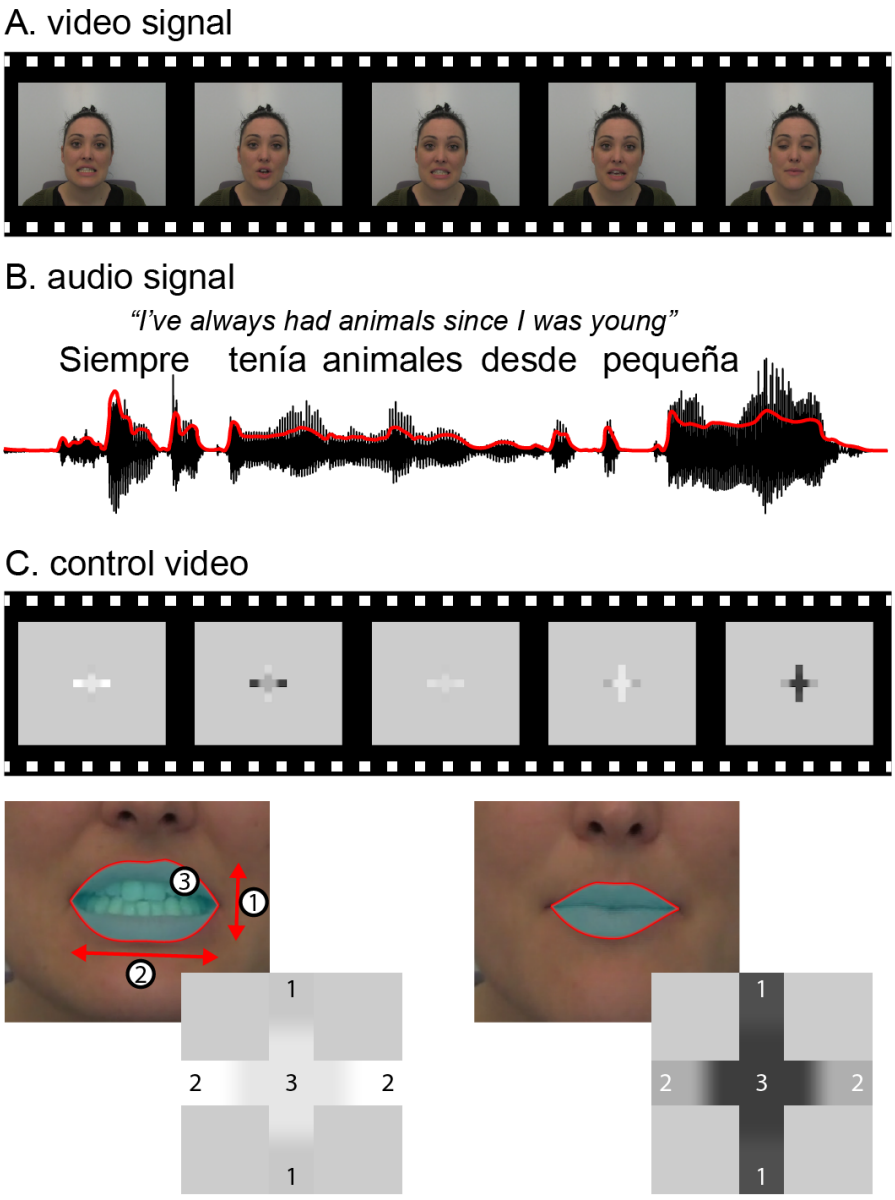

Figure 1. Experimental material. **A** and **B** — Two-second excerpt of video (**A**) and audio (**B**; auditory speech envelope in red) of the speaker telling a 5-min story about a given topic. There were 8 different videos. Video without sound was presented in *video-only*, and sound without video was presented in *audio-only*. **C** — Corresponding control video in which a

flickering Greek cross encoded speaker's mouth configuration. Based on a segmentation of mouth contours, the cross encoded mouth opening (1), mouth width (2), and mouth surface (3). The resulting video was presented in *control-video-only*.

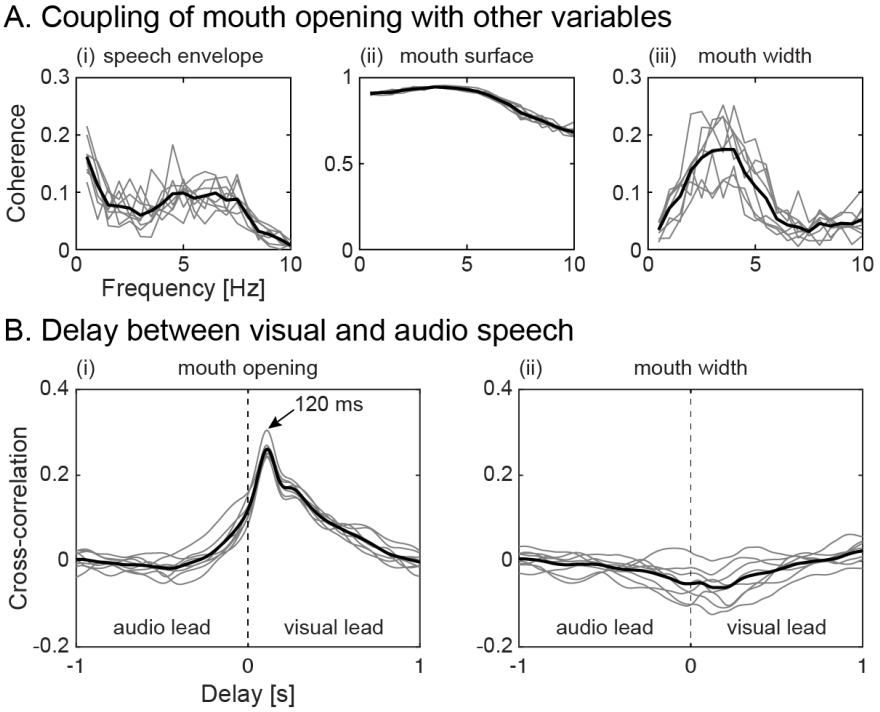

Figure 2. Relation between audio and visual speech signals. **A** — Frequency-dependent coupling (coherence) of mouth opening with auditory speech envelope (i), mouth surface (ii), and mouth width (iii). Coupling is quantified with coherence. There is one gray trace per video (8 in total), and thick black traces are the average across them all. **B** — Delay between visual and audio speech assessed with cross-correlation of auditory speech envelope with mouth opening (i) and mouth width (ii).

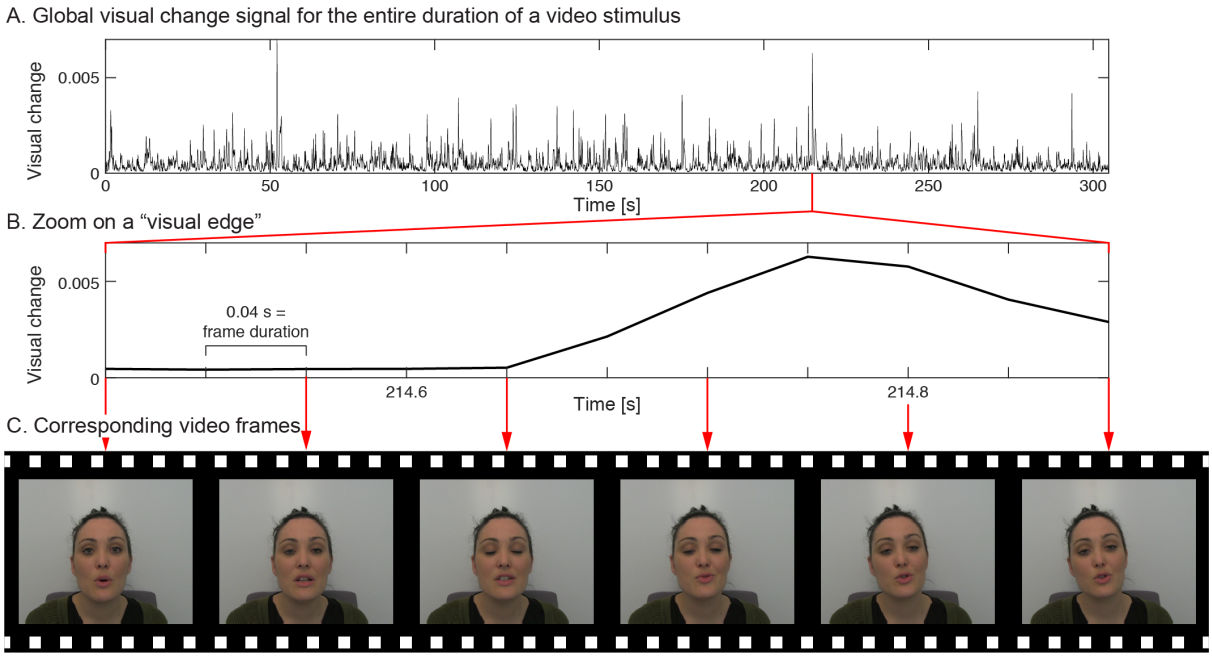

Figure 3. Global visual changes in the visual stimuli. **A** — The global visual change signal as a function of time for the entire duration of a video stimulus. **B** — Zoom on one of the most prominent edges (peaks) of the global visual change signal. **C** — Video frames corresponding to this visual edge, showing that it was due to head movements.

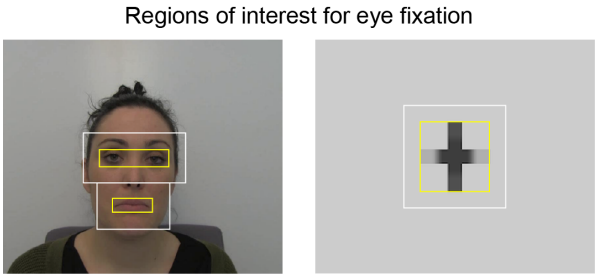

Figure 4. Regions of interest for eye fixation. The initial regions of interest are delineated in yellow, and the extended ones in white. Eye fixation analyses were based on extended regions. In *video-only* (*left*), the final region of interest comprised the mouth and the eyes. In control-video-only (*right*), it encompassed the flickering cross.

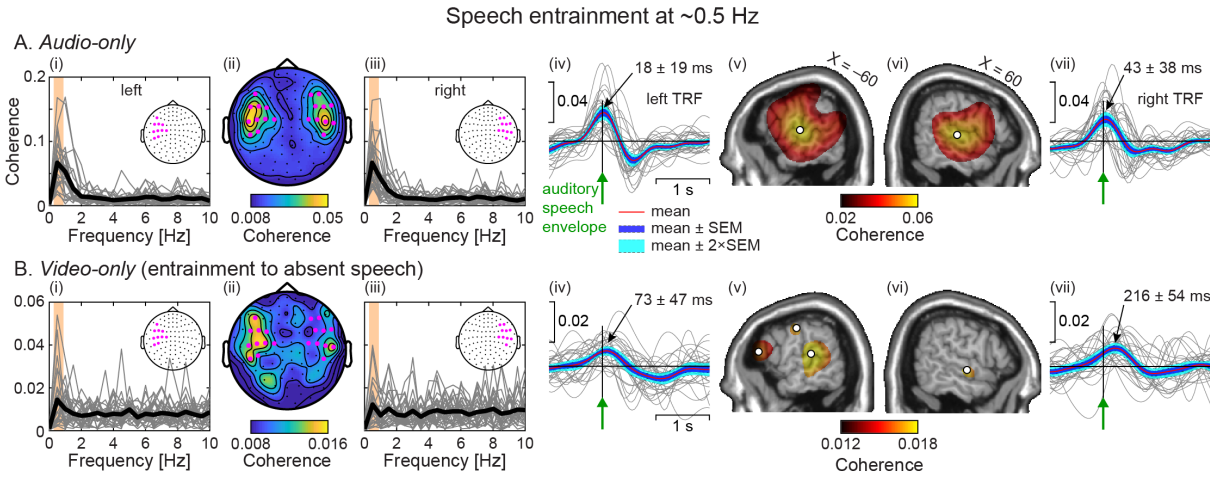

Figure 5. Speech entrainment at 0.5 Hz. **A** — Speech entrainment in *audio-only*. (i–iii) Sensor distribution of speech entrainment at 0.5 Hz quantified with coherence (ii) and its spectral distribution at a selection of 10 sensors in the left (i) and right hemisphere (iii) of maximal 0.5 Hz coherence (highlighted in magenta). Gray traces represent individual subject's spectra at the sensor of maximum 0.5 Hz coherence within the preselection, and the thick black trace is their group average. (iv–vii) Brain distribution of significant speech entrainment quantified with coherence in the left (v) and right hemispheres (vi) and the temporal response function (TRF) associated with auditory speech envelope at coordinates of peak coherence (marked with white discs) in the left (iv) and right hemispheres (vii). In brain images, significant coherence values at MNI coordinates |X| > 40 mm were projected orthogonally onto the parasagittal slice of coordinates |X| = 60 mm. **B** — Same as in **A** for *video-only*, illustrating that seeing speaker's face was enough to elicit significant speech entrainment at auditory cortices. Note that coherence spectra were estimated at the subject-specific sensor selected based on coherence in *audio-only*.

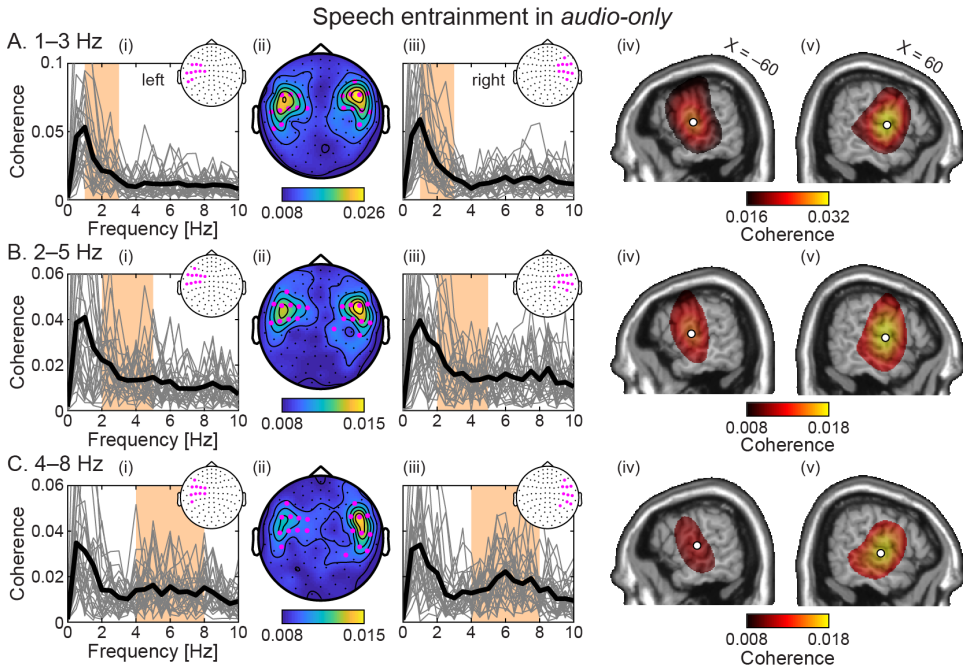

Figure 6. Speech entrainment quantified with coherence in *audio-only* at 1–3 Hz (**A**), 2–5 Hz (**B**) and 4–8 Hz (**C**). (i–iii) Sensor distribution of speech entrainment (ii) and its spectral distribution at a selection of 10 left- (i) and right-hemisphere (iii) sensors of maximum coherence (highlighted in magenta). Gray traces represent individual subject's spectra at the sensor of maximum coherence across the considered frequency range and within the preselection, and the thick black trace is their group average. (iv & v) Brain distribution of significant speech entrainment in the left (iv) and right hemispheres (v) produced as described in Fig. 5.

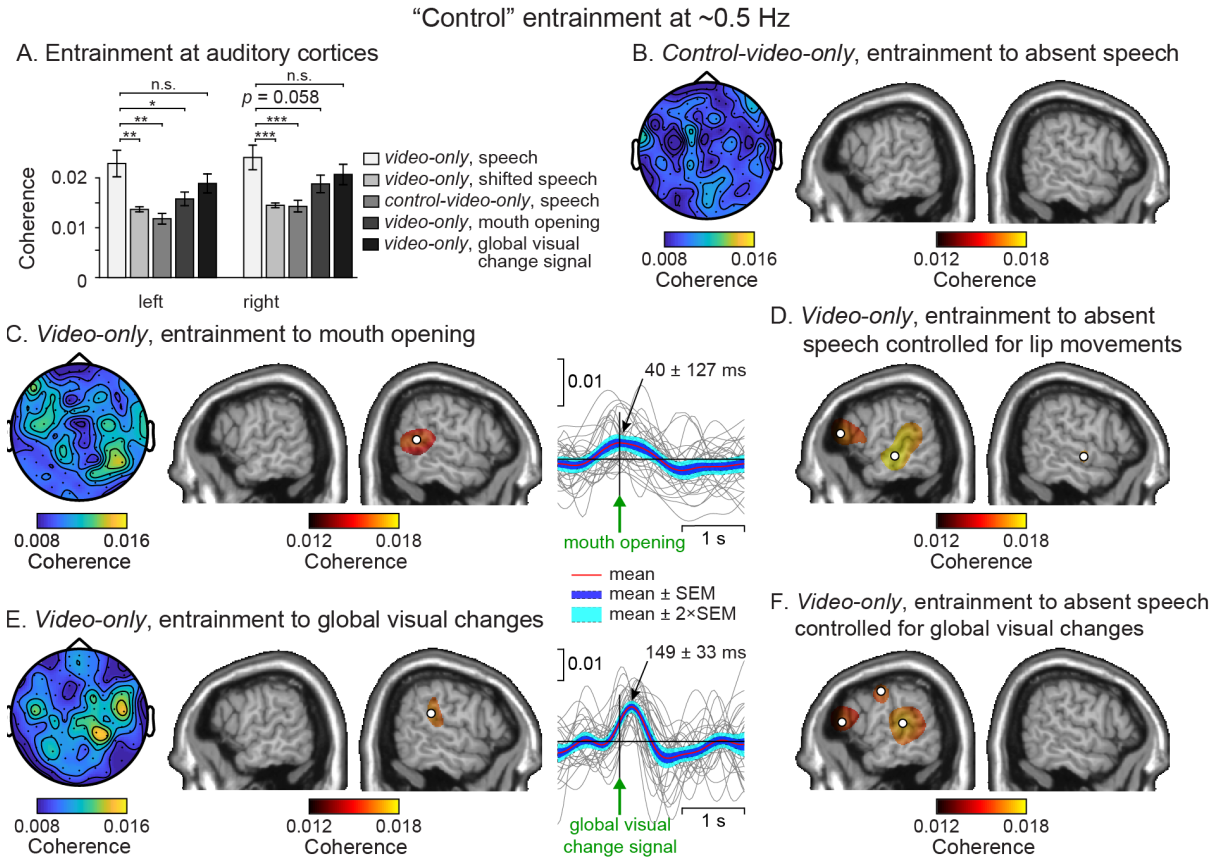

952

953 **Figure 7**. Control for the entrainment to absent speech at 0.5 Hz. **A** — Entrainment values
954 quantified with coherence at coordinates identified in *audio-only* (mean ± SD across
955 participants). **B** — Sensor and brain distribution of auditory speech entrainment in *control-*
956 *video-only* wherein speech entrainment was not significant. **C** — Sensor and brain
957 distribution of lip entrainment in *video-only* and associated temporal evolution. Lip
958 entrainment was significant only in the right angular gyrus. **D** — Brain distribution of
959 significant speech entrainment at 0.5 Hz after partialling out lip movements (mouth opening
960 and mouth width). **E** & **F** — As in C & D but for the global visual change signal instead of
961 mouth opening. Brain images were produced as described in Fig. 5.

962

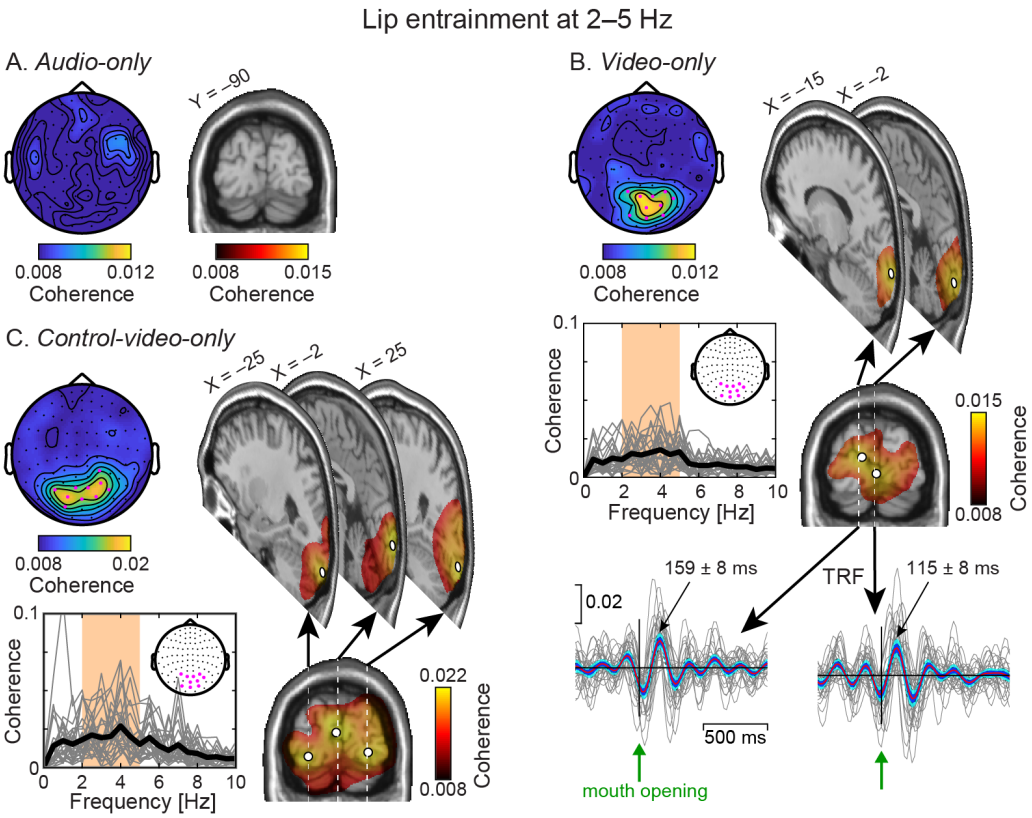

963

964 **Figure 8.** Lip entrainment at 2–5 Hz in *audio-only* (**A**), *video-only* (B) and *control-video-only*
965 (**C**). Lip entrainment is presented both in the sensor space and on the brain in all conditions
966 (*audio-only*, *video-only*, *control-video-only*). In brain maps, significant coherence values at
967 MNI coordinates Y < –70 mm were projected orthogonally onto the coronal slice of
968 coordinates |Y| = 90 mm. Locations of peak coherence are marked with white discs. Note that
969 coherence was not significant in *audio-only*. Additional parasagittal maps are presented for
970 all significant peaks of coherence. In these maps, the orthogonal projection was performed
971 for significant coherence values at Y coordinates less than 5 mm away from the selected slice
972 Y coordinate. The figure also presents a spectral distribution of coherence at a selection of 10
973 sensors of maximum 2–5 Hz coherence (highlighted in magenta) in *video-only* and *control-*
974 *video-only*. Gray traces represent individual subject's spectra at the sensor of maximum 2–5
975 Hz coherence within the preselection, and the thick black trace is their group average.
976 Finally, temporal response functions (TRF) to mouth opening are presented for the two
977 significant sources of peak entrainment to mouth opening in *video-only*.

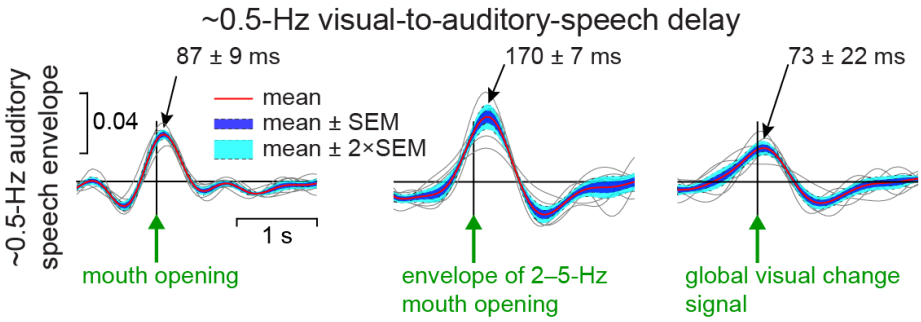

Figure 9. Visual-to-auditory-speech delays at ~0.5-Hz. Temporal response function of auditory speech envelope filtered through 0.2–1.5 Hz associated with the time course of mouth opening (*left*), 2–5-Hz envelope of mouth opening (*middle*), and global visual changes in video stimuli. There is one gray trace per video (8 in total), and thick red traces are the average across them all.